KSCE Journal of Civil Engineering (2019) 23(12):5002-5011

DOI 10.1007/s12205-019-2219-z

Geotechnical Engineering

pISSN 1226-7988, eISSN 1976-3808
www.springer.com/12205

A Pore Size Distribution-Based Microscopic Model for Evaluating the Permeability of Clay

Qian-Feng Gao*, Dan Zhao, Ling Zeng***, and Hui Dong******

Received November 18, 2018/Accepted September 15, 2019/Published Online October 24, 2019

Abstract

This work aimed to propose a semi-empirical model that predicts the permeability of saturated clay using the data of mercury intrusion porosimetry (MIP). First, the pore size distribution (PSD) curve obtained from an MIP test was regarded as a discrete probability function of pore diameters; thus, its shape could be characterized by probability parameters (e.g., the expected value and the standard deviation). Subsequently, these probability parameters, combined with the microporosity calculated from the volume of intruded mercury, were correlated with the permeability of clay based on Hagen-Poiseuille's equation. Next, the performance of the proposed permeability model was verified using data reported in the literature. Thereafter, the model was applied to estimate the permeability of normally consolidated (NC) and overconsolidated (OC) kaolin subjected to various triaxial loading. The results highlighted that the proposed model is capable of characterizing the sensitive variation of kaolin permeability under different overconsolidation ratios (OCRs), stress paths, and stress levels.

Keywords: *permeability model, pore size distribution, porosity, clay, mercury intrusion porosimetry, triaxial test*

1. Introduction

As one of the oldest building materials on Earth, clay usually serves as the base or even an essential part of buildings and structures. Moreover, since clay is relatively impermeable, it is also used as a natural barrier, such as in the cores of dams, in landfills and in nuclear waste storages, to prevent the seepage of water or toxic liquids (Delage *et al*., 2010). Therefore, it is important not only to determine the mechanical behavior of clay, but also to have a good knowledge of the clay permeability under various loading conditions.

Permeability describes how easily water can move through a porous medium. The laboratory methods used for measuring the permeability of clay include the falling-head permeability test, the indirect consolidation test, and the triaxial permeability test (Tavenas *et al*., 1983; Al-Tabbaa and Wood, 1987; Bello, 2013; Dong *et al*., 2017). However, the measured data often contain considerable measurement errors because of the extremely small order of magnitude of the data, leading to a large discrepancy between different testing methods. For this reason, many scholars have attempted to obtain the clay permeability from the theoretical point of view. The earlier theoretical and semi-empirical permeability model for porous media were usually developed based directly or indirectly on Hagen-Poiseuille's equation. These models commonly assume that porous media are a collection of straight, parallel, circular, and equal-sized capillaries and that the flow of water in them satisfies the laminar fluid flow. In practice, the above permeability models, especially the Kozeny-Carman model (Carman, 1956), are roughly valid for sands but not for clayey materials (Chapuis, 2012). To estimate the permeability of clay, some empirical permeability-porosity (or void ratio) relations have been proposed, such as the $\lg k - e$ relations proposed by Taylor (1948) and Nagaraj *et al.* (1993), the $\lg k - \lg e$ relation suggested by Mesri and Olson (1971) and the $k - e^c/(1+e)$ relation proposed by Samarasinghe *et al.* (1982). However, Tavenas *et al.* (1983) indicated that the permeability-porosity equations fail to consider the variation of pore sizes and none of them are generally valid for clays.

As technology advanced, many new techniques, such as mercury intrusion porosimetry (MIP), scanning electron microscopy (SEM) and X-ray computerized tomography (CT), for the quantification of soil micropores (≤ 10 μm) were introduced (Ninjgarav *et al*.,

*Lecturer, School of Traffic & Transportation Engineering, Changsha University of Science & Technology, Changsha 410114, China (E-mail: qianfeng.gao@csust.edu.cn)
**Lecturer, College of Civil Engineering and Architechture, Zhejiang University of Water Resources and Electric Power, Hangzhou 310018, China (E-mail: zhaodan1120@gmail.com)
***Associate Professor, School of Civil Engineering, Changsha University of Science & Technology, Changsha 410114, China (Corresponding Author, E-mail: zl001@csust.edu.cn)
****Associate Professor, Hunan Key Laboratory of Geomechanics and Engineering Safety, Xiangtan University, Xiangtan 411105, China (E-mail: donghui@xtu.edu.cn)

2007; Zuo *et al.*, 2016; Gao *et al.*, 2018; Zeng *et al.*, 2019). Microscopic experiments based on these high-tech approaches revealed that the microfabric and the micropore structure essentially control the permeability of soils (Li *et al.*, 2013; Yuan *et al.*, 2018; Gao *et al.*, 2019). This result prompted many researchers to focus on the correlation between soil permeability and various microstructural parameters (Garcia-Bengochea *et al.*, 1979; Juang and Holtz, 1986; Lapierre *et al.*, 1990; Schaap and Lebron, 2001; Gao and Hu, 2013; Ranaivomanana *et al.*, 2016). Among these, the relation between permeability and the pore size distribution (PSD) has become an issue of great concern. Garcia-Bengochea *et al.* (1979) defined a pore size parameter (PSP) based on the MIP results and proposed a power law between the PSP and the permeability of fine-grained soils. However, as Lapierre *et al.* (1990) commented, the model of Garcia-Bengochea *et al.* (1979) usually overestimates the permeability of clay and cannot give a unique function. Juang and Holtz (1986) developed a probability-based model to link the permeability of soil with the pore size density function. The pore size density function was deduced from the PSD data using the finite difference approximation and curve-fitting technique. Their model is able to predict the permeability of compacted soils well, whereas a function of pore size should be properly predetermined.

The objective of this work was to develop a general model for clay permeability considering the microporosity and the PSD. The PSD curve was considered as a discrete probability function of pore diameters; thus, its shape was characterized by the probability parameters (e.g., the expected value and the standard deviation). These probability parameters, combined with the microporosity, were correlated with the permeability of clay based on Hagen-Poiseuille's equation. The performance of the proposed model was verified using the data reported in the literature. Afterward, the model was used to estimate the permeability of remolded clay that triaxially sheared under different overconsolidation ratios (OCRs), stress paths, and stress levels. Therefore, the model's capability of determining the permeability of clay subjected to different triaxial loading conditions were evaluated.

2. Brief Description of the MIP Technique

The MIP technique is a widely used method for quantifying the pore structure of materials. It is based on the fact that a non-wetting liquid cannot intrude the pore space of a material until a sufficient pressure is applied. The relationship between the intrusion pressure and the pore size can be described by Washburn's equation:

$$D = -\frac{4\gamma\cos\theta}{P} \tag{1}$$

where D is the pore diameter; γ is the surface tension of the mercury; θ is the contact angle between the mercury and the pore wall; and P is the applied intrusion pressure of the mercury.

Therefore, by applying pressure incrementally to the mercury, one can obtain a sequence of pore diameters according to Eq. (1). Note that the MIP technique is based on the assumptions that the pores are cylindrical, the contact angle is constant, and the pore structure remains undamaged during the mercury intrusion. In addition, this technique is useful only for the measurement of pores open to the outside of a sample. This means that the microporosity yielded by MIP can be regarded as the effective porosity for fluid flow. Despite these limitations, many researchers have successfully characterized the PSD of clayey soils using this technique (Lapierre *et al.*, 1990; Delage *et al.*, 2010).

The results of the MIP tests are usually represented by the cumulative and differential curves of intruded volume per unit mass of the sample. If the pore diameters (D_i, i = 1, 2, 3, …, N) are successively numbered and the intervals of the logarithmic pore diameter ($\Delta\lg D_i$) are fixed, then the cumulative and differential volumes of the intruded mercury can be calculated by:

$$V_{\mathrm{Hg}} = \sum_{i=1}^{N} \Delta V_i \tag{2}$$

$$V_{\mathrm{diff},i} = \frac{\Delta V_i}{\Delta \lg D_i} \tag{3}$$

where V_{Hg} is the cumulative volume of the intruded mercury per unit sample mass; D_i is the median diameter of pore class i; ΔV_i is the volume increment of the intruded mercury per unit sample mass; and $V_{\mathrm{diff},i}$ is the differential volume of the intruded mercury per unit sample mass.

The cumulative and differential pore volume curves offer a wide range of information, including the total volume of the pores, the shape of the PSD, and the dominant pore diameter (D_0). By means of MIP, many experimental works indicated that the PSD curve of clays has either a bimodal form or a unimodal form (Delage and Lefebvre, 1984; Penumadu and Dean, 2000). To correlate the PSD with the permeability, it is necessary to characterize the shapes of the PSD curves. As presented previously, the pore diameters are calculated from a sequence of discrete mercury pressures; thus, the pore diameter can be considered as a discrete random variable. Therefore, the discrete probability function can be readily determined based on the PSD curve by (Juang and Holtz, 1986):

$$f(\lg D_i) = \frac{\Delta V_i}{V_{\mathrm{Hg}}} = \frac{V_{\mathrm{diff},i}}{V_{\mathrm{Hg}}}\Delta \lg D_i \tag{4}$$

$$\sum_{i=1}^{N} f(\lg D_i) = 1 \tag{5}$$

where f ($\lg D_i$) is the discrete probability function of pore diameters in a semi-logarithmic plane.

Figure 1 illustrates an example for the derivation of the discrete probability function using a unimodal PSD curve. For a good approximation of the discrete probability function, the interval of pore size classes, $\Delta\lg D_i$, has to be an appropriate constant. For the case given in Fig. 1, $\Delta\lg D_i = 0.1$ was used; thus, there were 60 equal-width classes (N = 60) in total, ranging from

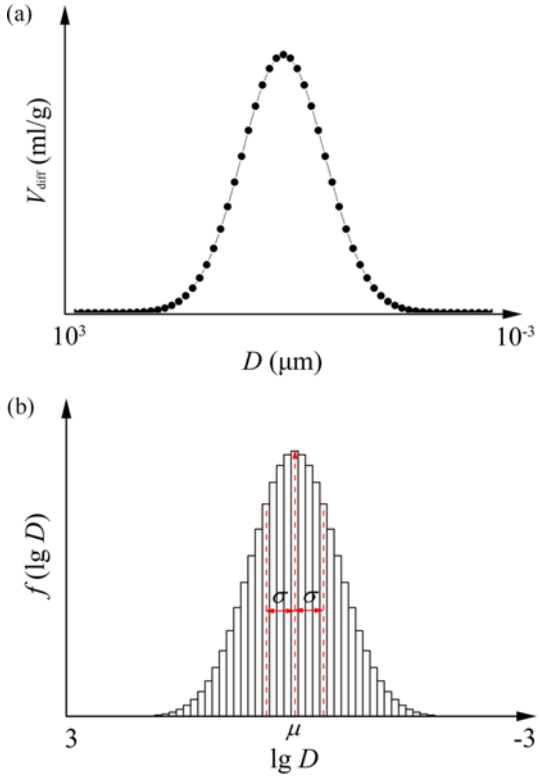

Fig. 1. Derivation of the Discrete Probability Function Using a Unimodal PSD Curve: (a) Differential Pore Volume, (b) Probability Function

1 nm up to 1 mm. Therefore, one can characterize the PSD curve using the expected value and the standard deviation, which are expressed by:

$$\mu=\sum_{i=1}^{N} f(\lg D_i)\cdot \lg D_i \tag{6}$$

$$\sigma=\sqrt{\sum_{i=1}^{N}(\lg D_i-\mu)^2\cdot f(\lg D_i)} \tag{7}$$

where μ and σ are the expected value and the standard deviation of the logarithmic pore diameter, respectively.

3. Microscopic Permeability Modelling of Clay

3.1 New Permeability Model using MIP Data

The new permeability model is primarily based on Hagen-Poiseuille's equation. For a porous medium assembled from a series of parallel, circular, and identical capillaries, its permeability can be calculated using the following equation (Leonards, 1962):

$$k=\frac{\gamma_w n}{32\eta_w}D^2 \tag{8}$$

where k is the coefficient of permeability; γ_w is the specific weight of water; n is the porosity; D is the diameter of the capillary; and η_w is the dynamic viscosity of water.

Since the isolated pores do not contribute to the permeability of clay, while the pore size distribution has a significant influence on the permeability, Eq. (8) was modified as follows:

$$k=\frac{\gamma_w n^*}{32\eta_w}D^{*2} \tag{9}$$

where n^* is the effective microporosity; and D^* is the effective pore diameter.

n^* and D^* are expressed by:

$$n^*=e_{MIP}/(1+e_{MIP}) \tag{10}$$

$$D^*=c\cdot D_e \tag{11}$$

where e_{MIP} is the void ratio calculated using the MIP data; c is a non-dimensional correction factor related to the PSD; and D_e is the expected pore diameter.

e_{MIP} and D_e can be further calculated by:

$$e_{MIP}=V_{Hg}\cdot\rho_s \tag{12}$$

$$D_e=10^{\mu} \tag{13}$$

where ρ_s is the mass density of a soil solid.

Substituting Eq. (10) and Eq. (11) into Eq. (9) yields:

$$k=\frac{c^2\gamma_w}{32\eta_w}\cdot\frac{e_{MIP}}{1+e_{MIP}}\cdot D_e^{\,2} \tag{14}$$

Note that the larger the value of μ, the larger the expected pore diameter, then the greater the soil permeability. Thus, there is a positive correlation between μ and k. On the other hand, the larger the value of σ, then the smaller the number of medium pores and the greater the number of small and large pores considering constant microporosity and expected pore diameter. Although the small increase in large pores is conducive to the permeability, the great reduction in medium pores must lead to a notable decrease in soil permeability. Thus, a negative correlation between σ and k is assumed. Based on the above analysis, the following expression that links the non-dimensional factor (c) to μ and σ is proposed for clay:

$$c=m\cdot\sqrt{\frac{\mu+3}{\sigma}} \tag{15}$$

where m is a model constant.

If Eq. (15) is substituted for c in Eq. (14), the permeability model becomes:

$$k=\frac{m^2\gamma_w}{32\eta_w}\cdot\frac{e_{MIP}}{1+e_{MIP}}\cdot\frac{\mu+3}{\sigma}\cdot D_e^2 \tag{16}$$

Equation (16) can be rewritten as:

$$k=C_m\cdot\frac{e_{MIP}}{1+e_{MIP}}\cdot\frac{\mu+3}{\sigma}\cdot D_e^2 \tag{17}$$

$$C_m=\frac{m^2\gamma_w}{32\eta_w} \tag{18}$$

where C_m is a model constant related to the fluid property and pore shape.

3.2 Parametric Interpretation and Analysis

The proposed permeability model has two variables, i.e., c and D_e, which are dependent on two probability parameters (i.e., μ and σ) of the PSD curve. As is known, μ controls the skewness of the probability function curve, while σ determines the kurtosis of the probability function curve (Fig. 1(b)). Accordingly, the variation of the PSD curve is characterized by c and D_e. D_e is a function of μ; thus, it controls the skewness of the PSD curve. By contrast, c is a function of μ and σ; thus, it plays two major roles. On the one hand, the numerator of c considers the sensitivity of the permeability to pore diameters. On the other hand, the denominator of c governs the kurtosis of the PSD curve.

Figure 2 shows the relationship between the variation of the probability function curve (or the PSD curve) and the model parameters. In the first case (Fig. 2(a)), the three clay samples have identical PSD shapes but different expected pore diameters. This difference leads to the distinct permeability of the material: A sample whose expected pore diameter is larger has a greater permeability. In the second case (Fig. 2(b)), the three clay samples have the same expected pore diameter; however, the PSD shapes are different (more precisely, the kurtosises are different). According to the permeability model, the higher the kurtosis, the greater the value of c and thus the larger the permeability.

A parametric study was conducted to quantitatively examine the behavior of the proposed model. The results are presented in Fig. 3. One can note that as μ increases from -2.0 to 1.2 (i.e., D_e varies from 10 nm to 15.8 μm), the permeability increases by 7 orders of magnitude. On the other hand, the permeability decreases greatly as σ increases from zero to 0.3, but the reduction trend slows down as σ further increases. In addition, the parameter m also affects the permeability, but its influence decreases as its value increases, especially when m becomes larger than 0.20.

3.3 Verification of the Permeability Model

In this section, the proposed permeability model was verified using the MIP data and permeability reported in the literature. The test data were obtained for a mixture of natural silt and commercial kaolin (Garcia-Bengochea, 1978), intact and remolded Louiseville clay (Lapierre *et al.*, 1990), and three types of clay from China (Kong, 2007; Zhou, 2013), as listed in Table 1. Since the PSD curves given in the above literature had different pore diameter intervals ($\Delta \lg D_i$) and some curves were even presented without symbols, all of them were converted into the same system with $\Delta \lg D_i = 0.1$. An example of the operation is presented in Fig. 4. Fig. 4(a) presents the original data reported by Garcia-Bengochea (1978); each original PSD curve had 22 data points. As shown in Fig. 4(b), 38 extra points were added to each curve to convert the data into a system of 60 equal-width classes. Note that the shape of the PSD curve and the total pore volume (V_{Hg}) were unchanged before and after the conversion. In this case, the discrete probability function of every sample can be obtained using the method illustrated in Fig. 1.

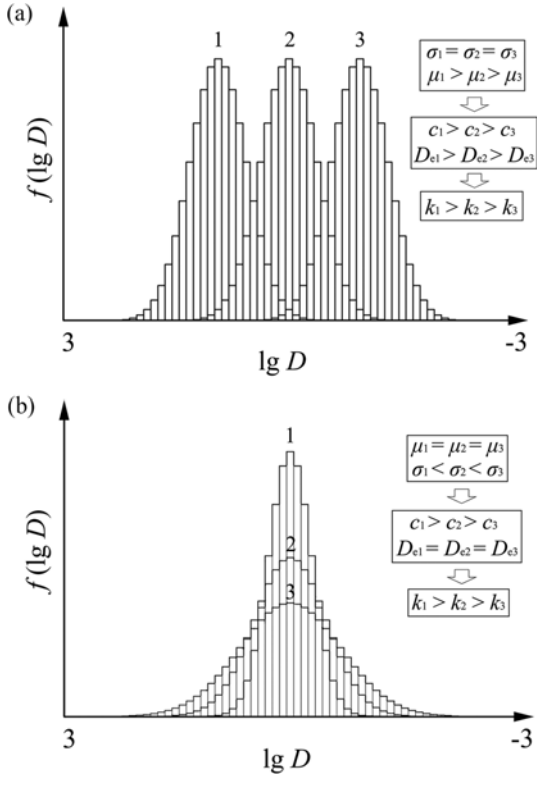

Fig. 2. Relationship between the Shape of the PSD and the Model Parameters: (a) Change in Skewness, (b) Change in Kurtosis

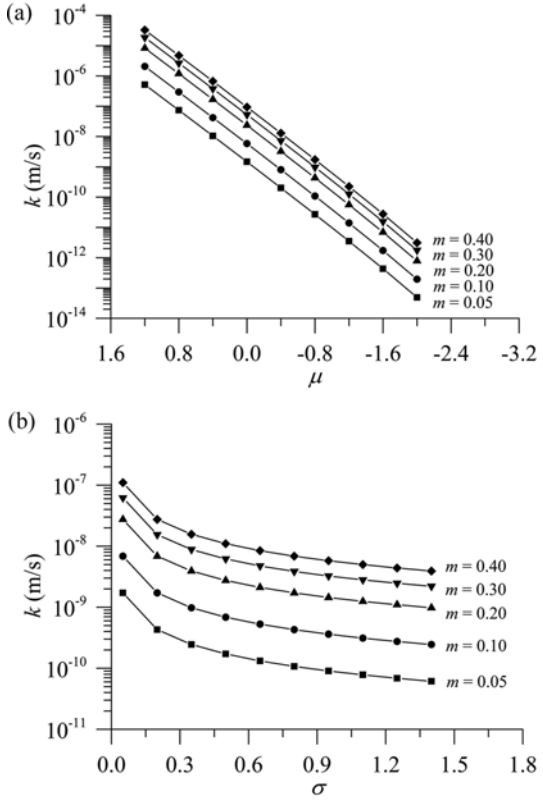

Fig. 3. Parametric Analysis of the Proposed Permeability Model (e_{MIP} = 0.8): (a) Influence of μ, (b) Influence of σ

Table 1. Dataset Used for the Verification of the Proposed Permeability Model

Data source	(1) Garcia-Bengochea (1978)			(2) Lapierre *et al.* (1990)		(3) Zhou (2013)		(4) Kong (2007)
Data number	5	9	6	6	5	5	5	5
Material	50% silt + 50% kaolin	70% silt + 30% kaolin	90% silt + 10% kaolin	Intact Louiseville clay	Remolded Louiseville clay	Guangzhou (GZ) clay	Shenzhen (SZ) clay	Shanghai (SH) clay
Specific gravity	2.69	2.71	2.72	–	–	2.60	2.60	2.65
Liquid limit	37%	25%	–	68%	64%	43%	45%	52%
Plastic limit	27%	18%	–	30%	28%	23%	20%	26%
Range of e_{MIP}	0.56–0.72	0.41–0.64	0.44–0.59	0.98–1.93	0.93–1.79	1.19–1.82	0.99–1.44	0.42–0.80
Range of k_m ($\times 10^{-9}$ m/s)	0.6–740.0	0.4–160.0	5.0–390.0	0.1–0.9	0.05–0.8	2.8–11.0*	2.0–4.5*	1.13–15.6

*The mean value of the measured permeabilities (k_m) in the horizontal and vertical directions.

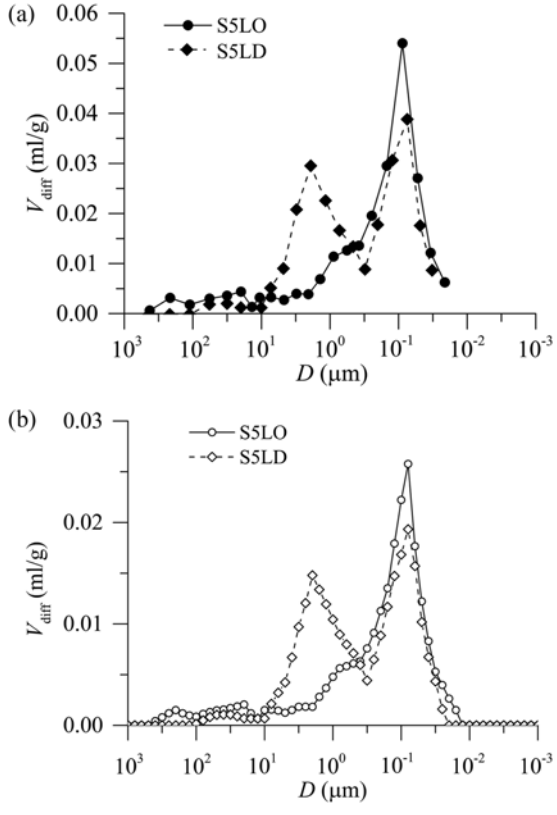

Fig. 4. Conversion of Original Curve to Curve with 60 Equal-Width Classes: (a) Original Data, (b) Converted Data

Figure 5 compares the measured permeability (k_m) and the calculated permeability (k_c) using the proposed model. The permeability calculated using the lg$k$ – e relation was also presented for comparison purposes. The order of the permeability of the examined fine-grained soils varies from 5×10^{-11} m/s up to 7×10^{-7} m/s. One can note that the model proposed in this paper appropriately predicts the permeability of Louiseville clay, Guangzhou clay, Shenzhen clay and Shanghai clay, with minor errors. However, the predicted results of the silt-kaolin mixture using the proposed model do not agree very well with the measured data, especially for the mixtures with a high percentage of silt. In addition, when the permeability is greater than 10^{-7} m/s, the consistency is rather bad; however, in this case, the performance

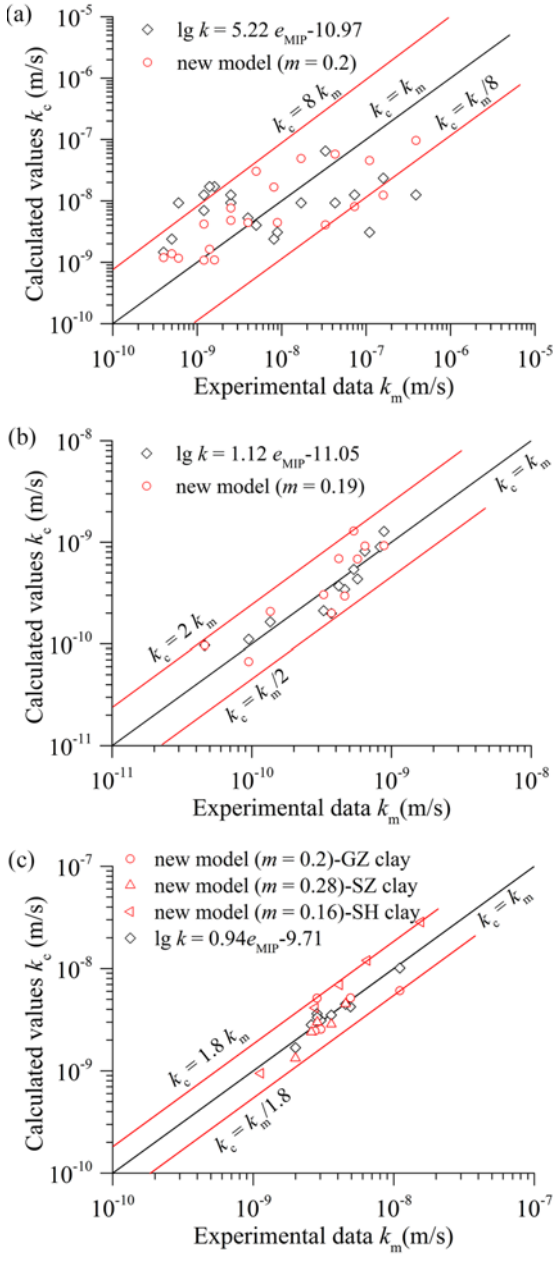

Fig. 5. Verification of the Proposed Permeability Model: (a) Silt-kaolin Mixtures, (b) Louiseville Clay, (c) Guangzhou Clay, Shenzhen Clay and Shanghai Clay

of the proposed model is still better than that of the lg$k$ – e relation. Therefore, it may be concluded that the proposed model is only suitable for clays, whose permeability is less than 10^{-7} m/s; for other types of soil, different forms of Eq. (15) must be developed. Compared to the lg$k$ – e relation, the obvious advantage of the new model is that its form does not change between clays, and the variation range of the constant m is limited. In the cases shown in Fig. 5, the value of m changes from 0.16 to 0.28; thus, it can be approximately taken as 0.2.

4. Application of the Permeability Model to Kaolin under Triaxial Loading

In this section, the proposed permeability model was adopted to calculate the permeability of a commercial kaolin subjected to various triaxial loading using the MIP data. The liquid limit and plastic limit of the material are 42% and 21%, respectively, and the specific gravity of the soil solids is 2.63.

4.1 Mechanical Behavior of Kaolin

The consolidated drained (CD) triaxial compression tests were carried out on both normally consolidated (NC) and overconsolidated (OC) remolded kaolin specimens considering two different stress paths: the conventional constant σ'_3 stress path (S) and the constant p' stress path (P). Triaxial shearing was terminated when the stress level reached the predesigned point P2 (p'_2 = 300 kPa, q_2 = 150 kPa) or P3 (p'_3 = 300 kPa, q_3 = 257 kPa) in the (p', q) plane. The specifications of the triaxial tests are summarized in Table 2, where p'_1 is the isotropic conslidation stress, e_{00} is the initial void ratio, e_0 is the void ratio after isotropic consolidation, and e_f is the void ratio at the end of triaxial shearing. Noted that the measured void ratios (e_0) were slightly scattered around the compression line (C_c = 0.29) or the swelling line (C_s = 0.05) due to the variation of the initial void ratios (e_{00}) when using the consolidation method to form specimens. Therefore, a translation was performed to restrict the measured void ratios from evolving from the compression line for the NC specimens and from the swelling line for the OC specimens during triaxial shearing. After the translation, the following relation was obtained: $e' = e + \Delta e$ (e' is the translated void ratio; e is the measured void ratio; and Δe is the deviation of e_0 from the compression line or the swelling line).

The results of triaxial tests are illustrated in Fig. 6. Fig. 6(a) shows that the stress-strain relationships were slightly affected by stress paths but significantly affected by OCRs and stress levels. The lg p' – e' curves in Fig. 6(b) shows that during triaxial shearing, the void ratios of the OCR3.3_P300_P2 and OCR3.3_P300_P2 specimens on the constant p' stress path slightly increased exhibiting dilative behavior. By contrast, the void ratios of the remaining specimens including the OCR4.0_S250_P2 specimen decreased showing contractive behavior.

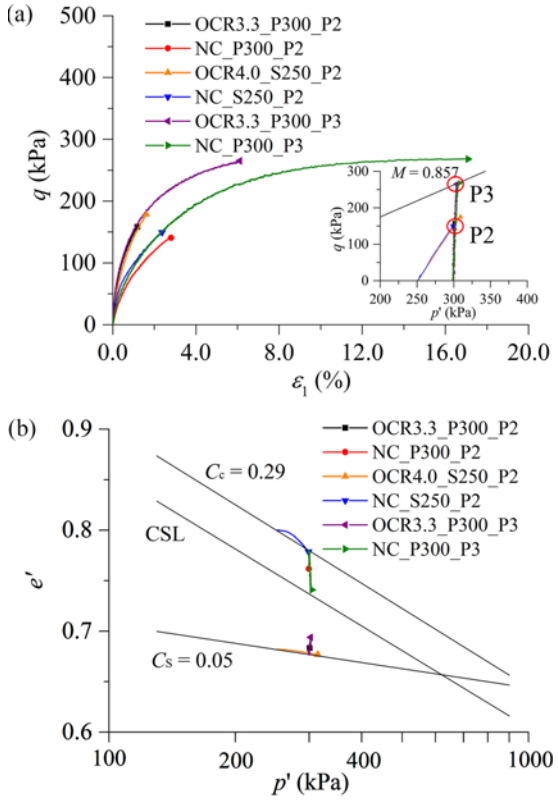

Fig. 6. Triaxial Test Results of Remolded Kaolin Specimens: (a) ε_1 – q Curves, (b) lgp'-e' Curves

4.2 PSD and Microporosity Via MIP

After the mechanical testing, the MIP tests were conducted on the small cubic samples that extracted from cylindrical specimens.

Figure 7 presents the differential pore volumes versus pore diameters of different clay specimens. One can note that the shape of the PSD curves, particularly the height of the peak points, was affected by stress paths, stress levels and OCRs. It shows that the pore diameters of all specimens had a wide range, from 6 nm up to 100 μm. It is noted that more than 80% of the total pore volume measured via the MIP tests fell within the pore

Table 2. Triaxial Tests on Remolded Kaolin Specimens

Specimen	OCR	Stress path	Stress level	p'_1 (kPa)	e_{00}	e_0	e_f	Δe
NC_P300_P2	1.0	P	P2	300	0.893	0.758	0.738	0.022
NC_S250_P2	1.0	S	P2	250	0.921	0.790	0.766	0.010
NC_P300_P3	1.0	P	P3	300	0.930	0.776	0.735	0.004
OCR3.3_P300_P2	3.3	P	P2	300	0.966	0.727	0.741	-0.050
OCR4.0_S250_P2	4.0	S	P2	250	0.809	0.608	0.604	0.074
OCR3.3_P300_P3	3.3	P	P3	300	0.965	0.723	0.753	-0.046

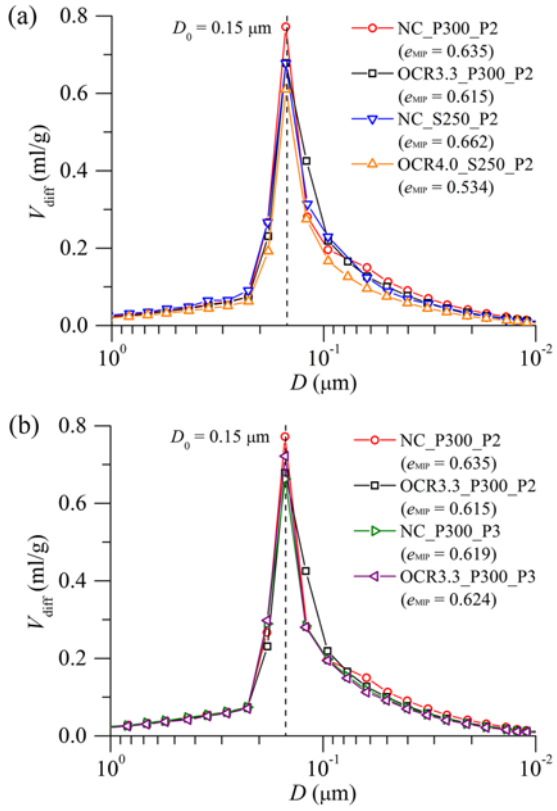

Fig. 7. Differential Pore Volume versus Pore Diameter: (a) Influence of Stress Paths, (b) Influence of Stress Levels

size range of 0.03 μm to 0.35 μm. Furthermore, the dominant pore diameters (D_0) of these specimens were all approximately 0.15 μm.

In addition, comparing the microvoid ratio measured via MIP (e_{MIP}, see Fig. 7) with the macrovoid ratio obtained from the conventional tests (e_f, see Table 2), one can note that the microvoid ratio was significantly smaller than the macrovoid ratio. The major reason must be that the MIP technique does not take into account the isolated pore volumes in specimens.

As stated previously, a translation of the macrovoid ratios was performed to eliminate the initial errors (Fig. 6(b)). Similarly, the microvoid ratios also need to be corrected to generalize the results. Herein, the following relation between the deviations (Δe_{MIP} and Δe) of the microvoid ratio and the macrovoid ratio was assumed: $\Delta e_{MIP}/e_{MIP} = \Delta e/e_f$. Thus, the corrected microvoid ratio is expressed by $e'_{MIP} = e_{MIP} + \Delta e_{MIP} = e_{MIP}(1 + \Delta e/e_f)$. The corrected microvoid ratio and macrovoid ratio are presented in Fig. 8.

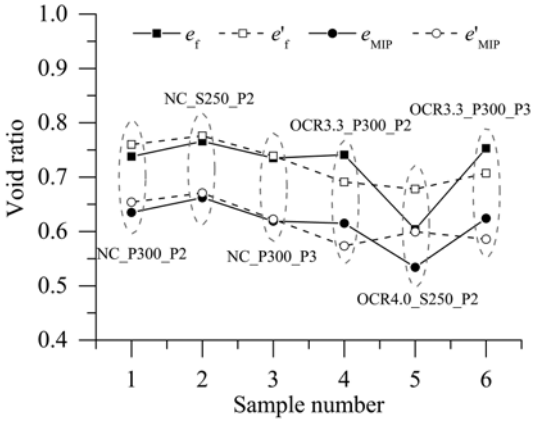

Fig. 8. Corrected Microvoid Ratios and Macrovoid Ratios

4.3 Predicted Coefficients of Permeability

4.3.1 Characteristic Parameters of PSD Curves

The probability parameters (e.g., μ and σ) and other model parameters related to the PSD were calculated and are listed in Table 3.

It appears that at the P2 stress level the values of μ of the NC_S250_P2 and OCR4.0_S250_P2 specimens were larger than those of the NC_P300_P2 and OCR3.3_P300_P2 specimens, respectively. This means that when a specimen is sheared on the constant σ'_3 stress path, the tail of the PSD curve on the large-diameter side is longer or fatter than that of a specimen on the constant p' stress path. Furthermore, the values of σ of the NC_S250_P2 and OCR4.0_S250_P2 specimens were also greater than those of the NC_P300_P2 and OCR3.3_P300_P2 specimens, indicating that the PSD curves of the specimens on the constant σ'_3 stress path had lower kurtoses than those of the specimens on the constant p' stress path.

A considerable influence of OCRs on the PSD shape is observed. At the P2 stress level, the values of μ of the NC specimens (e.g., NC_P300_P2 and NC_S250_P2) were larger than those of the OC specimens (e.g., OCR3.3_P300_P2 and OCR4.0_S250_P2). Whereas, the value of μ of the NC_P300_P3 specimen was slightly smaller than that of the OCR3.3_P300_P3 specimen. The value of σ of the NC_S250_P2 specimen was visibly greater than that of the OCR4.0_S250_P2 specimen. By contrast, the values of σ of the NC_P300_P2 and NC_P300_P3 specimens were less than those of the OCR3.3_P300_P2 and OCR3.3_P300_P3 specimens, respectively.

Table 3. Characteristic Parameters of the PSD Curves

Specimen	OCR	Stress path	Stress level	D_0 (μm)	μ	σ	D_e (μm)	c	D^* (μm)
NC_P300_P2	1.0	P	P2	0.150	-0.860	0.453	0.138	0.435	0.060
NC_S250_P2	1.0	S	P2	0.150	-0.807	0.557	0.156	0.397	0.062
NC_P300_P3	1.0	P	P3	0.150	-0.862	0.460	0.137	0.431	0.059
OCR3.3_P300_P2	3.3	P	P2	0.150	-0.888	0.454	0.129	0.431	0.056
OCR4.0_S250_P2	4.0	S	P2	0.150	-0.854	0.476	0.140	0.424	0.059
OCR3.3_P300_P3	3.3	P	P3	0.150	-0.854	0.479	0.140	0.423	0.059

One can note that, on a given stress path, the values of μ of the NC_P300_P2 and NC_P300_P3 specimens were approximated, while the value of μ of the OCR3.3_P300_P2 specimen was significantly smaller than that of the OCR3.3_P300_P3 specimen. The values of σ of the specimens at the P2 stress level were visibly smaller than those of the corresponding specimens at the P3 stress level, indicating that the PSD was wider when a specimen was subjected to a higher stress level.

It is also observed that the values of D^* of the NC_P300_P2 and NC_S250_P2 specimens were greater than those of the OCR3.3_P300_P2 and OCR4.0_S250_P2 specimens, respectively. This is reasonable because the pores of the OC specimens were more compressed than those of the NC specimens. However, the value of D^* of the OCR3.3_P300_P3 specimen was equal to that of the NC_P300_P3 specimen, which was probably due to the volumetric dilation that developed in the OC specimen.

4.3.2 Predicted Coefficients of Permeability

Table 4 gives the predicted coefficients of permeability of six specimens using the proposed permeability model with $m = 0.2$. In Table 4, n^* is the microporosity calculated based on the measured microvoid ratio (e_{MIP}). $n^{*\prime}$ is the microporosity calculated based on the corrected microvoid ratio (e'_{MIP}) (see Fig. 8). k and k' are the coefficients of permeability calculated using n^* and $n^{*\prime}$, respectively. To further verify the reliability of the proposed permeability model, the coefficients of permeability (k_m) of two kaolin specimens (i.e., Oed_200 and Oed_1000) indirectly evaluated by oedometer tests at vertical effective stresses of 200 kPa and 1,000 kPa and those (k) calculated from the MIP data of the specimens by the proposed model are also presented. The results show that the predicted coefficients of permeability of the two oedometer specimens are acceptably consistent with the measured data, suggesting that the proposed permeability model is indeed applicable to kaolin.

One can note that the correction operation is meaningful, as it makes the results more reasonable. After the correction, the kaolin specimens under the tested loading conditions had small permeabilities varying from 3.4×10^{-10} m/s to 4.7×10^{-10} m/s (Fig. 9). It is observed that the permeability of the NC_P300_P2 specimen was greater than that of the OCR3.3_P300_P2 specimen. Similar trends were also found among the other four specimens. These results reflect an accepted fact that the OC clay is more impermeable than the NC clay.

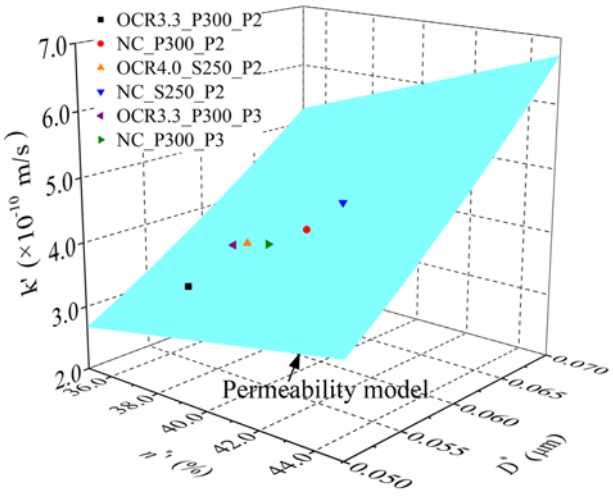

Fig. 9. Predicted Coefficients of Permeability of Remolded Kaolin Specimens

On the other hand, the permeabilities of the specimens on the constant p' stress path were smaller than those of the specimens on the constant σ_3' stress path, although all the specimens had the same stress level. For instance, the permeability of the NC_P300_P2 specimen was 4.363×10^{-10} m/s, which was significantly less than that of the NC_S250_P2 specimen. This is likely because the specimens on the constant p' stress path encountered larger confining pressure at the beginning of triaxial shearing compared to those on the constant σ_3' stress path.

In addition, one can note that a higher stress level led to a smaller permeability for the NC specimens (e.g., NC_P300_P2 and NC_P300_P3). This result agrees well with the findings of Lei *et al.* (2016). By contrast, a higher stress level usually resulted in a greater permeability for the OC specimens because of the increasing dilatancy phenomenon.

Therefore, it may be concluded that the permeability of clays was sensitive to the triaxial loading conditions, including the stress history (OCR), the stress path, and the stress level. The model proposed in this paper was capable of characterizing these complex features of clay permeability.

5. Conclusions

In this work, a semi-empirical model for the permeability of remolded clay was proposed using the PSD and the microporosity

Table 4. Predicted Coefficients of Permeability of Six Kaolin Specimens

Specimen	OCR	Stress path	Stress level	n^* (%)	$n^{*\prime}$ (%)	D^* (μm)	k ($\times 10^{-10}$ m/s)	k' ($\times 10^{-10}$ m/s)	k_m ($\times 10^{-10}$ m/s)
NC_P300_P2	1.0	P	P2	38.8	39.5	0.060	4.285	4.363	—
NC_S250_P2	1.0	S	P2	39.8	40.1	0.062	4.660	4.697	—
NC_P300_P3	1.0	P	P3	38.2	38.4	0.059	4.094	4.108	—
OCR3.3_P300_P2	3.3	P	P2	38.1	36.4	0.056	3.622	3.467	—
OCR4.0_S250_P2	4.0	S	P2	34.8	37.5	0.059	3.750	4.037	—
OCR3.3_P300_P3	3.3	P	P3	38.4	36.9	0.059	4.117	3.958	—
Oed_200	—	—	—	40.9	—	0.084	8.893	—	15.749
Oed_1000	—	—	—	33.5	—	0.031	0.991	—	1.206

obtained via the MIP technique. The PSD curve was considered as a discrete probability function of pore diameters; thus, its shape was characterized by the probability parameters (e.g., the expected value and the standard deviation). These probability parameters were then used to quantify the effective pore diameter. Based on Hagen-Poiseuille's equation, the effective pore diameter and the microporosity were correlated to the permeability of clays. The proposed permeability model may be expressed in the following form:

$$k = C_m \cdot \frac{e_{MIP}}{1+e_{MIP}} \cdot \frac{\mu+3}{\sigma} \cdot D_e^2 \tag{19}$$

This model was verified using the measured data of the silt-kaolin mixture, the intact and remolded Louiseville clay, and three types of clay from China, all of which were reported in the literature. The verification results demonstrated that the proposed model could appropriately predict clay permeabilities ranging from 10^{-11} m/s to 10^{-7} m/s. Then, the permeability model was applied to estimate the permeability of remolded kaolin subjected to various triaxial loading. The following conclusions may be drawn based on the analyses of the results:

1. The influence of different triaxial loading conditions on the microvoid ratio is significant. However, their influence on the shape of the PSD curve is usually not very obvious. In this case, the probability parameters were helpful in quantifying the small changes in the PSD shape.
2. The proposed model was capable of evaluating the average coefficients of permeability of kaolin under various triaxial loading conditions. However, the model cannot consider the anisotropy of clay permeability because the MIP technique fails to quantify the anisotropy of pore structures.

Acknowledgements

This work was supported by the National Natural Science Foundation of China (Nos. 51838001, 51878070, 51878078) and the Hunan Key Laboratory of Geomechanics and Engineering Safety, China (No. 16GES04). The authors appreciate the help of Dr. Lamine Ighil-Ameur with regard to triaxial testing.

ORCID

Qian-Feng Gao https://orcid.org/0000-0003-4844-2345
Dan Zhao https://orcid.org/0000-0003-1084-7726
Ling Zeng https://orcid.org/0000-0001-8167-1049
Hui Dong https://orcid.org/0000-0001-6597-9588

References

Al-Tabbaa, A. and Wood, D. M. (1987). "Some measurements of the permeability of kaolin." *Geotechnique*, Vol. 37, No. 4, pp. 499-514, DOI: 10.1680/geot.1987.37.4.499.

Bello, A. A. (2013). "Hydraulic conductivity of three compacted reddish brown tropical soils." *KSCE Journal of Civil Engineering*, Vol. 17, No. 5, pp. 939-948, DOI: 10.1007/s12205-013-0155-x.

Carman, P. C. (1956). *Flow of gases through porous media*, Butterworths, London, UK.

Chapuis, R. P. (2012). "Predicting the saturated hydraulic conductivity of soils: A review." *Bulletin of Engineering Geology and the Environment*, Vol. 71, No. 3, pp. 401-434, DOI: 10.1007/s10064-012-0418-7.

Delage, P., Cui, Y. J., and Tang, A. M. (2010). "Clays in radioactive waste disposal." *Journal of Rock Mechanics and Geotechnical Engineering*, Vol. 2, No. 2, pp. 111-123, DOI: 10.3724/SP.J.1235.2010.00111.

Delage, P. and Lefebvre, G. (1984). "Study of the structure of a sensitive Champlain clay and of its evolution during consolidation." *Canadian Geotechnical Journal*, Vol. 21, No. 1, pp. 21-35, DOI: 10.1139/t84-003.

Dong, H., Huang, R., and Gao, Q. F. (2017). "Rainfall infiltration performance and its relation to mesoscopic structural properties of a gravelly soil slope." *Engineering Geology*, Vol. 230, pp. 1-10, DOI: 10.1016/j.enggeo.2017.09.005.

Gao, Q. F., Dong, H., Huang, R., and Li, Z. F. (2019). "Structural characteristics and hydraulic conductivity of an eluvial-colluvial gravelly soil." *Bulletin of Engineering Geology and the Environment*, Vol. 78, No. 7, pp. 5011-5028, DOI: 10.1007/s10064-018-01455-1.

Gao, Z. and Hu, Q. (2013). "Estimating permeability using median pore-throat radius obtained from mercury intrusion porosimetry." *Journal of Geophysics and Engineering*, Vol. 10, No. 2, DOI: 10.1088/1742-2132/10/2/025014.

Gao, Q. F., Jrad, M., Ighil Ameur, L., Hattab, M., and Fleureau, J. M. (2018). "Dilatancy phenomenon study in remolded clays - A micro-macro investigation." *Proceedings of China-Europe Conference on Geotechnical Engineering*, Springer, Cham, Switzerland, pp. 148-152.

Garcia-Bengochea, I. (1978). *The relation between permeability and pore size distribution of compacted clayey silts*, MScE Thesis and Joint Highway Research Project Report, Purdue University, West Lafayette, IN, USA.

Garcia-Bengochea, I., Altschaeffl, A. G., and Lovell, C. W. (1979). "Pore distribution and permeability of silty clays." *Journal of the Geotechnical Engineering Division*, Vol. 105, No. 7, pp. 839-856.

Juang, C. H. and Holtz, R.D. (1986). "A probabilistic permeability model and the pore size density function." *International Journal for Numerical and Analytical Methods in Geomechanics*, Vol. 10, No. 5, pp. 543-553, DOI: 10.1002/nag.1610100506.

Kong, L. R. (2007). *Microstructural behavior of saturated soft clay and an elasto-plastic constitutive model considering microstructure*, PhD Dissertation, Tongji University, Shanghai, China (in Chinese).

Lapierre, C., Leroueil, S., and Locat, J. (1990). "Mercury intrusion and permeability of Louiseville clay." *Canadian Geotechnical Journal*, Vol. 27, No. 6, pp. 761-773, DOI: 10.1139/t90-090.

Lei, H., Wu, Y., Yu, Y., Zhang, B., and Lv, H. (2016). "Influence of shear on permeability of clayey soil." *International Journal of Geomechanics*, Vol. 16, No. 5, DOI: 10.1061/(ASCE)GM.1943-5622.0000636.

Leonards, G. A. (1962). *Foundation Engineering*, McGraw-Hill, New York, NY, USA.

Li, Z., Katsumi, T., Inui, T., and Takai, A. (2013). "Fabric effect on hydraulic conductivity of kaolin under different chemical and biochemical conditions." *Soils and Foundations*, Vol. 53, No. 5, pp. 680-691, DOI: 10.1016/j.sandf.2013.08.006.

Mesri, G. and Olson, R. E. (1971). "Mechanisms controlling the permeability of clays." *Clays and Clay Minerals*, Vol. 19, No. 3, pp. 151-158,

DOI: 10.1346/CCMN.1971.0190303.

Nagaraj, T. S., Pandian, N. S., and Narasimha-Raju, P. S. R. (1993). "Stress state permeability relationships for fine-grained soils." *Géotechnique*, Vol. 43, No. 2, pp. 333-336, DOI: 10.1680/geot.1993.43.2.333.

Ninjgarav, E., Chung, S. G., Jang, W. Y., and Ryu, C. K. (2007). "Pore size distribution of Pusan clay measured by mercury intrusion porosimetry." *KSCE Journal of Civil Engineering*, Vol. 11, No. 3, pp. 133-139, DOI: 10.1007/BF02823892.

Penumadu, D. and Dean, J. (2000). "Compressibility effect in evaluating the pore-size distribution of kaolin clay using mercury intrusion porosimetry." *Canadian Geotechnical Journal*, Vol. 37, No. 2, pp. 393-405, DOI: 10.1139/t99-121.

Ranaivomanana, H., Razakamanantsoa, A., and Amiri, O. (2016). "Permeability prediction of soils including degree of compaction and microstructure." *International Journal of Geomechanics*, Vol. 17, No. 4, DOI: 10.1061/(ASCE)GM.1943-5622.0000792.

Samarasinghe, A. M., Huang, Y. H., and Drnevich, V. P. (1982). "Permeability and consolidation of normally consolidated soils." *Journal of the Geotechnical Engineering Division*, Vol. 108, No. 6, pp. 835-850.

Schaap, M. G. and Lebron, I. (2001). "Using microscope observations of thin sections to estimate soil permeability with the Kozeny–Carman equation." *Journal of Hydrology*, Vol. 251, No. 3, pp. 186-201, DOI: 10.1016/S0022-1694(01)00468-1.

Tavenas, F., Leblond, P., Jean, P., and Leroueil, S. (1983). "The permeability of natural soft clays. Part I: Methods of laboratory measurement." *Canadian Geotechnical Journal*, Vol. 20, No. 4, pp. 629-644, DOI: 10.1139/t83-072.

Taylor, D. W. (1948). *Fundamentals of soil mechanics*, John Wiley & Sons, New York, USA.

Yuan, S. Y., Liu, X. F., and Buzzi, O. (2018). "Effects of soil structure on the permeability of saturated Maryland clay." *Géotechnique*, Vol. 69, No. 1, pp. 72-78, DOI: 10.1680/jgeot.17.p.120.

Zeng, L., Liu, J., Gao, Q. F., and Bian, H. (2019). "Evolution characteristics of the cracks in the completely disintegrated carbonaceous mudstone subjected to cyclic wetting and drying." *Advances in Civil Engineering*, Vol. 2019, Article ID 1279695, pp. 1-10, DOI: 10.1155/2019/1279695.

Zhou, H. (2013). *Study on soft soil microstructure and mechanism of seepage and consolidation in Pearl River Delta (PRD)*, PhD Dissertation, South China University of Technology, Guangzhou, China (in Chinese).

Zuo, C., Liu, D., Ding, S., and Chen, J. (2016). "Micro-characteristics of strength reduction of tuff residual soil with different moisture." *KSCE Journal of Civil Engineering*, Vol. 20, No. 2, pp. 639-646, DOI: 10.1007/s12205-015-0408-y.